Atomic Structure of Quantum Gold Nanowires: Quantification of the Lattice Strain

Paromita Kundu,[†,*] Stuart Turner,[†] Sandra Van Aert,[†] N. Ravishankar,[‡] and Gustaaf Van Tendeloo[†]

[†]Electron Microscopy for Materials Science (EMAT), University of Antwerp, Groenenborgerlaan 171, 2020 Antwerp, Belgium and [‡]Materials Research Center, Indian Institute of Science, Bangalore, India 560012

ABSTRACT Theoretical studies exist to compute the atomic arrangement in gold nanowires and the influence on their electronic behavior with decreasing diameter. Experimental studies, *e.g.*, by transmission electron microscopy, on chemically synthesized ultrafine wires are however lacking owing to the unavailability of suitable protocols for sample preparation and the stability of the wires under electron beam irradiation. In this work, we present an atomic scale structural investigation on quantum single crystalline gold nanowires of 2 nm diameter, chemically prepared on a carbon film grid. Using low dose aberration-corrected high resolution (S)TEM, we observe an inhomogeneous strain distribution in the crystal, largely concentrated at the twin boundaries and the surface along with the presence of facets and surface steps leading to a noncircular cross section of the wires. These structural aspects are critical inputs needed to determine their unique electronic character and their potential as a suitable catalyst material. Furthermore, electron-beam-induced structural changes at the atomic scale, having implications on their mechanical behavior and their suitability as interconnects, are discussed.

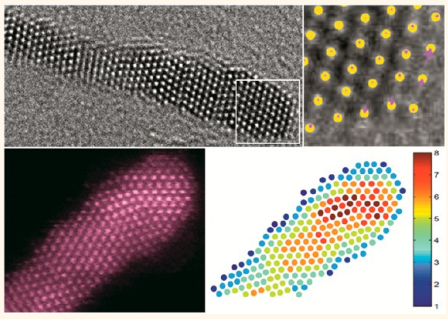

KEYWORDS: Au nanowires · ultrafine · aberration-corrected microscopy · surface strain · 3D atomic structure

Nanoscale gold has been a material of interest for decades owing to its large and controllable variation of functionality depending on its shape, form and size.[1−3] It has been exploited suitably in various fields of application including catalysis, optics, plasmonics and biotechnology.[4−6] Gold nanowires of molecular scale dimensions are of fundamental as well as technological interest owing to their tunable electrical transport characteristics which can lead to ballistic conduction. Theoretical models predict the onset of quantized conductance upon decrease of the wire diameter and a deviation of its structure from bulk, implying a structural dependence on the electron transport characteristics.[7,8] This quantization effect due to downsizing is a direct consequence of their electronic states which are dependent on their atomic structure. These tunable electronic properties open up possibilities for the exploitation of Au nanostructures as highly active catalysts[9,10] and sensors, where the mechanism is electron sensitive[11] and structure dependent.[12] Several protocols are reported for wire synthesis in solution;[13−16] however, exploring/exploiting them remained challenging until the growth of single crystal ultrafine wires (∼2 nm diameter) with [111] growth direction could be achieved in a controlled way on various substrates.[17] This controlled synthesis allowed to probe the electronic properties of such fine wires and it was demonstrated that ultrathin Au nanowires of ∼2 nm diameter exhibit an insulating state, unlike metallic bulk Au, due to a strongly correlated electron transport mechanism.[18] However, a detailed structural investigation has not been reported to date. Atomic level defects acting as scattering barriers[19] or any morphological changes induced by interaction with the substrate could largely influence the electron transport behavior.[20,21] Besides, surface strain can be induced in the crystal upon downsizing, influencing its electronic properties and hence its catalytic behavior as demonstrated for twinned Au nanoparticles.[22] It is therefore essential to investigate the stability and structural characteristics of these

* Address correspondence to paromita.kundu@uantwerp.be.

Received for review October 7, 2013 and accepted November 29, 2013.

Published online November 29, 2013
10.1021/nn4052315

wires down to an atomic scale. This not only is of fundamental interest, but also provides critical insights into its potential as a promising molecular scale electronic material for different applications.

Aberration-corrected Scanning Transmission Electron Microscopy ((S)TEM) is a state-of-art technique to investigate crystal structures and extract information atom-by-atom.[23] Before aberration-correction was implemented in TEM, it was necessary to obtain a phase image by exit wave reconstruction, enabling the elimination of, *e.g.*, delocalization effects in the amplitude image due to lens aberrations, to obtain a precise determination of atomic column positions.[24] With the onset of aberration correction, atomic columns can be imaged at their correct positions for extremely thin specimens like nanowires, allowing atomic column positions to be estimated directly from the acquired HRTEM images, without the need for a through focal series and exit wave reconstruction. We exploit this technique to thoroughly investigate the atomic structure of the ~2 nm thin gold nanowires. The extreme fragility and beam sensitivity of the wires make structural characterization by microscopy challenging; however, with low dose and an energy filtered mode of operation, it has been possible to obtain atomic resolution and quantification of the deviations from the bulk FCC lattice. The beam-induced structural changes are, on the one hand undesirable, but on the other hand, they provide information on the stability and the bonding in such ultrasmall systems. They are important in understanding the mechanical behavior of the wires. High-angle annular dark field STEM (HAADF-STEM) imaging has been performed on the wires to confirm the external morphology as well as the internal atomic structure; it reveals the presence of atomic scale surface steps and the presence of distinct facets leading to a noncircular cross section.

RESULTS AND DISCUSSION

The molecular scale wires of 2 nm diameter were grown directly on a carbon film (~3 nm thick in the thinnest areas) coated on a Cu mesh grid following a protocol described in our recent report.[17] In this case, the grid was placed on a 1 cm × 1 cm glass slide and covered with Teflon tape to leave only a portion of carbon exposed to the reaction medium. Oleyl amine reduces Au(III) precursor to Au(0) which nucleates in the medium and on the carbon film. We followed the method in which an intermediate cleaning step for the substrate is involved after nucleating the Au particles at 95 °C;[25] this removes the excess oleyl amine on the substrate and leaves a monolayer capping on the Au particles. The substrate with Au was redipped in the solution containing fine Au particles and the wire growth takes place by an oriented attachment mechanism in this step when ascorbic acid is added at 40 °C. This protocol leads to pristine wires suited for high resolution (S)TEM imaging which otherwise is difficult with wires grown in solution and drop cast on grid, as it is not possible to clean them off the surfactants without damaging the wires, for this kind of study. The challenging issue while studying the wires in TEM mode was to obtain sufficient contrast at low dose from the resolved wires due to the presence of the carbon background. Therefore, the experiment was carried out in energy filtered mode, using a 30 eV slit centered around the zero-loss peak to reduce the contribution from plasmons and other inelastic scattering effects, and enhance the contrast in the HRTEM images. All TEM imaging was performed on a TITAN^3 microscope, equipped with an aberration corrector for both TEM and STEM mode and operated at 120 kV. This acceleration voltage of 120 kV was selected as a trade-off between stability of the nanowires under electron beam (lowered knock-on damage) and the need for high image resolution. To maximize the stability of the nanowires under the electron beam, a low dose of approximately 20 e/Å^2 s (screen current of 45 pA) was used for high resolution TEM imaging (see movie in Supporting Information, S1). In STEM mode, a convergence semiangle α of 21 mrad was used, and an acceptance semiangle β of 85 mrad to guarantee HAADF (Z-contrast) conditions. Figure 1 shows the as-grown wires on the carbon support (Figure 1a) and high resolution images of the wires from different regions. The images presented here are recorded under overfocus conditions, imaging the atomic column positions as bright dots; this is confirmed by simulated HR images for the microscope under similar conditions (see Supporting Information, Figure S2). From the high resolution images in Figure 1b–d, it is clear that the wires preferentially grow along the [111] orientation.

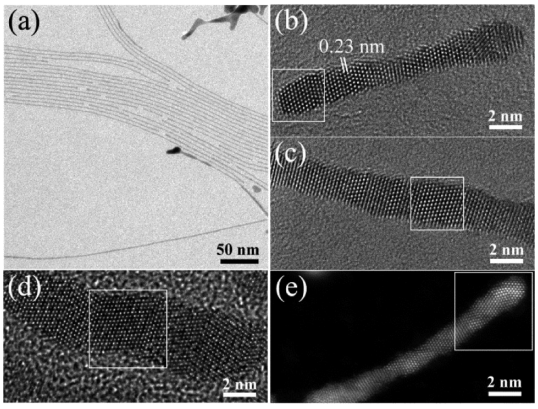

Figure 1. (a) Bright field TEM image of a bunch of ultrafine Au nanowires grown directly on a thin carbon film. (b–d) High resolution aberration-corrected TEM micrographs of (b) a thin wire end, (c) middle, and (d) a thicker wire segment, respectively. In all cases, the growth direction is [111] as confirmed from the *d*-spacing of 2.3 Å along the length. Under the overfocus imaging conditions used, the Au atomic columns are imaged as bright contrast. (e) High resolution HAADF-STEM image of a wire segment. The regions considered for quantitative analysis are marked with white boxes in the respective figures.

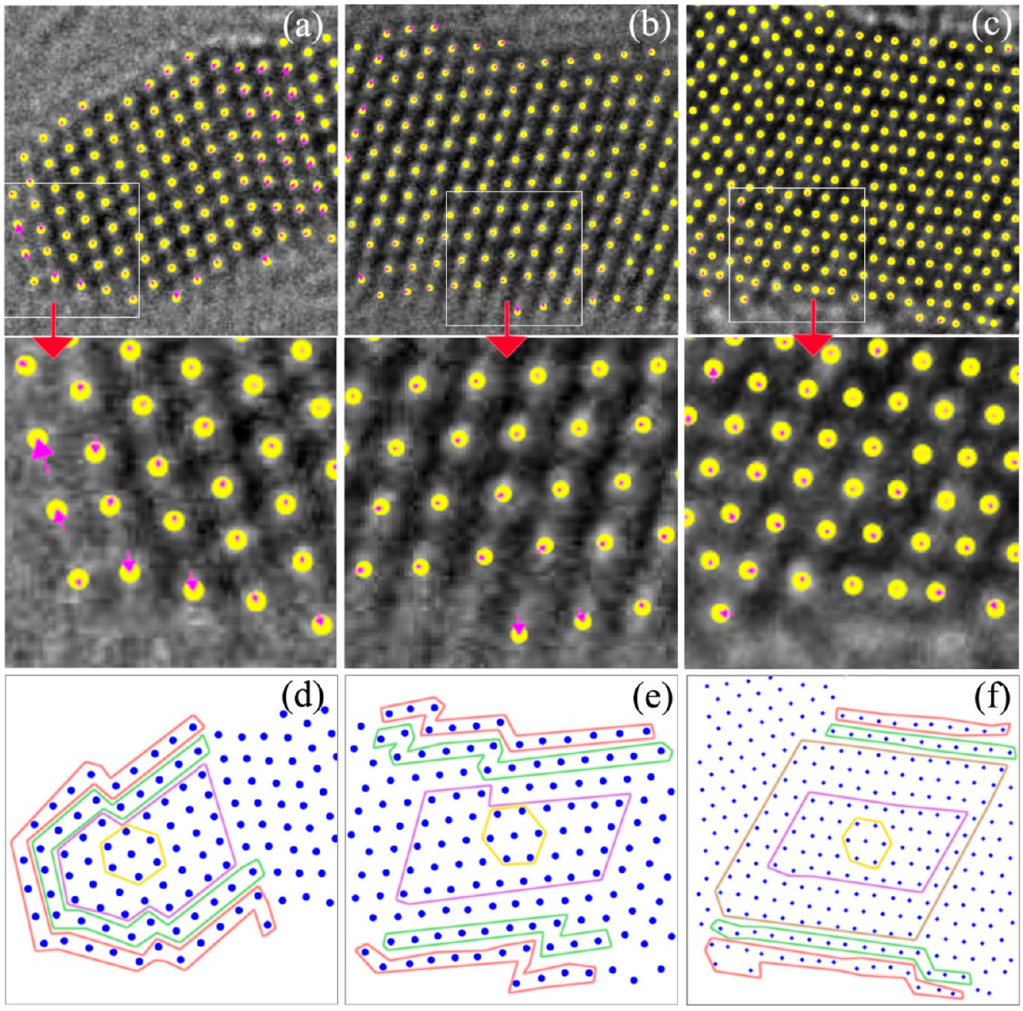

Figure 2. High resolution images of an end (a), mid- (b), and thicker (c) wire segment with estimated positions of atomic columns (yellow dots) and their relative displacements (pink arrows; the tails of the arrows are at the perfect atomic positions corresponding to the extended fcc lattice and the arrow-heads terminate at the estimated column positions). A magnified view of a selected portion of each wire segment is presented as adjoined figures below. (d–f) The estimated position plots corresponding to the images in (a–c), demarking the set of atomic columns considered for calculating the mean displacements. The columns bound in red are the outermost layer of atomic columns, those bound in green are in the second outermost layer, those bound in violet make out the innermost core (5 atomic columns wide), and those in yellow mark the 7 neighboring atomic columns chosen to construct the reference lattice. In (f), the brown zone denotes the core (11 atomic columns wide) leaving out only the outer two layers.

However, most of the wires do not completely lie in the [1$\bar{1}$0] zone orientation; some regions of the wires are visibly rotated around the [111] growth axis. This suggests that the wires have a slightly twisted geometry, which is also apparent from the HRSTEM image shown in Figure 1e. A similar morphology is predicted by theoretical models in this size regime and shown experimentally for wires created under the microscope by stretching or beam etching from a thin film of gold;[26–28] however, those wires have a different orientation than the chemically grown wires discussed here. The entire length of the wire contains a large amount of parallel (111) twin boundaries separated by only a few atomic planes. Such twin defects are expected due to the oriented attachment of the faceted cuboctahedral particles during wire growth.[13] We analyzed three distinct, well resolved portions of wires: an end-segment, a midsegment and a thicker wire segment (~ 4 nm diameter) as marked in Figure 1. Although aberration-corrected TEM significantly improves the visual interpretability of the images, quantitative numbers for the atomic column positions are not readily available. To overcome this problem, statistical parameter estimation theory is known to be an extremely powerful technique.[24,29–31] With this technique, a parametric model describing the experimental images as a superposition of Gaussian peaks located at the atomic column positions can be assumed. The parameters of this model, including the atomic column positions, can then be determined using the least-squares estimator. The estimated atomic column positions are indicated by means of yellow dots in Figure 2a–c. To evaluate possible displacements of the atomic positions, an fcc reference lattice has been

TABLE 1. Mean Displacement Values (in pm), with Error Bars Indicated Therein, of the Estimated Atomic Column Positions of the Au Wires from a Perfect fcc Lattice Resembling Bulk

wire portion analyzed	thin (∼2 nm) END-segment	thin (∼2 nm) MID-segment	thick (∼4 nm) MID-segment
Reference consisting of 7 neighboring columns	6.7 ± 0.8	4.6 ± 0.8	8.8 ± 2
Outermost layer	55.1 ± 4.8	45.1 ± 4.2; 50.9 ± 5.7	29.3 ± 4.7; 36.3 ± 4.4
Second outermost layer	27 ± 2.7	29.9 ± 4.1; 30.9 ± 2.8	18.9 ± 3.7; 24.3 ± 3.1
Inner core (5 atomic columns wide)	18.4 ± 1.6	11.3 ± 0.1	12.3 ± 1.2
Inner core (11 atomic columns wide)	-	-	16.9 ± 1

constructed along the [1$\bar{1}$0] zone-axis. To do so, a set of parameters defining this lattice has been estimated from atomic columns in the center such that the overall displacement is smallest (∼(6−8) ± 2 pm). The 7 neighboring columns indicated by the yellow contour in Figure 2d−f have been chosen as a reference. To illustrate this, Figure S3 (Supporting Information), corresponding to Figure 2a, shows the estimated positions and the positions resulting from an extended lattice in yellow and green dots, respectively, as an example. In this manner, the displacements of the estimated atomic columns with respect to the perfect lattice configuration can be indicated as shown in Figure 2a−c. The displacements have been marked by arrows with the arrows pointing from the positions of the columns at the ideal lattice sites toward the estimated positions marked in yellow. The mean displacement is measured for the inner core consisting of 4−5 columns across the width of the wire (region marked by the purple contour), for the outermost shell (marked by the red contour) and for the second outermost shell of columns (marked by the green contour) as indicated in Figure 2d−f, and the displacement values are compiled in Table 1 for different cases. In all cases, the columns are largely displaced, by ∼55 ± 5 pm (end-segment), ∼(45−50) ± 5 pm (midsegment) and ∼(30−36) ± 4 pm (thicker wire) from their actual position in the outermost layer of the wire which could be a strong effect due to interaction with the electron beam and the fact that they are less coordinated to the inner core. However, there is a significant displacement of the second layer as well which is ∼30 ± 3 pm for the thinner wire segments (corresponding to the end-segment and midsegment in this case) and ∼20 ± 3 pm for the thicker wire. Considering the inner core of 4−5 atomic columns in each case, the mean displacement is relatively more for the end-segment (∼18 ± 2 pm) than the other two cases (∼11 ± 1 pm). For the thicker segment when we consider a larger area as the inner core (leaving out only the outermost two shells), the mean displacement increases to ∼17 ± 1 pm. This implies that the deviation is mostly at the surface layers and increases outward. We can refer to this effect as strain in the crystal which increases significantly at the outer few layers of atoms and also it is larger at the tip of the wires (Figure 2a). The results are consistent with the presence of a surface stress leading to displacements that decrease as one goes into the bulk from the surface.

It is interesting to observe the direction of the displacements which indicates predominantly an expansion of the lattice outward but random at the surface layers. The shift, however, is larger and more prominent at the twin boundaries (marked in Figure S3 in Supporting Information) and it deviates largely from the ideal configuration if we extend the lattice geometrically by mirroring at the twin boundary as in Figure 2a. The direction of displacement indicates a transverse shear accompanied by a longitudinal stretch in the wire at the different twin interfaces. This experimental configuration closely resembles theoretical models and structures obtained by stretching/e-beam etching of a thin gold film as mentioned earlier.[28] In those cases, the wire orientation was [110] with approximately 1 nm cross section, whereas we have 2−3 nm diameter wires grown chemically in the [111] direction at a large scale. We have also analyzed individual segments across the twin planes choosing the reference column in the respective segment as shown in Figure 3a. Here the nature of the displacement is identical in each segment as discussed before; however, the two ideal extended lattices do not merge at the twin plane, confirming a shear of the (111) atomic plane at the twin boundary (inset of Figure 3a showing the twin boundary). This also clarifies our previous discussion on the significant unidirectional shift observed when a mathematical/geometrical twin was introduced. This shearing of the (111) planes is clearly evident at the break junction as well as in Figure 3b, which is acquired after allowing the break junction to form under the influence of the e-beam.

The wire tips are faceted and contain a large density of surface steps along the entire length as is clear from the high resolution images. The presence of a corrugated surface with few atom steps is evident from the analysis of the aberration corrected HAADF-STEM image (obtained with less than 40 pA current to prevent beam damage and structural changes) shown in Figure 4a (tip portion of the wire in Figure 1e). The atom counting method, reported earlier for different types of nanoparticles, is employed to compute the cross-sectional geometry which normally cannot be obtained from high resolution 2D projection TEM images.[32−36]

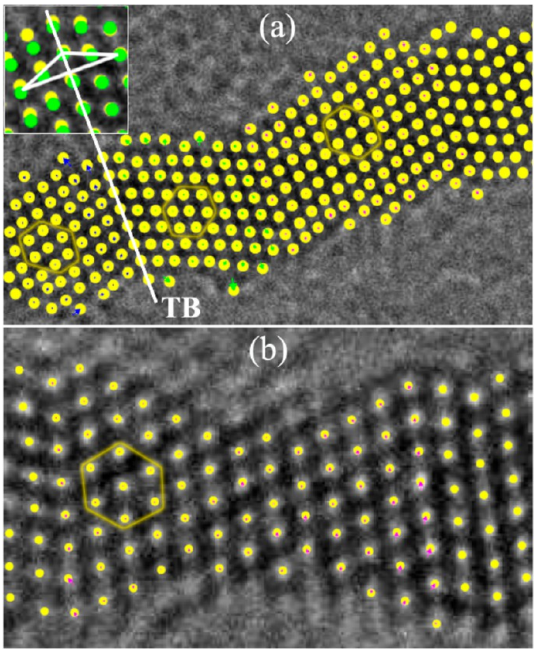

Figure 3. High resolution TEM images with estimated atomic column positions (yellow dots) and displacement from the extended FCC lattice (pink arrows) of (a) a wire segment with multiple twins which is analyzed choosing independent references, as marked with yellow lined region, in each of the portions separated by a twin boundary. Inset shows a selected region (where the ideal lattice and estimated atomic column positions are marked with green and yellow dots, respectively) around the twin boundary (TB) marked with a white line and extended to the inset and (b) a wire portion with a break junction created under the beam with the reference as indicated.

To determine the number of Au atoms in each atomic column, the column intensities in the HRSTEM image have been determined using a model-based approach[37] in which it is taken into account that they scale with the number of atoms in the column. Next, the statistically meaningful column types with a different number of Au atoms were determined. The resulting image with precise atom counts is given in Figure 4b showing the least count of 1 atom at the surface and 6−8 atoms at the core.

Assuming a perfect fcc lattice *d*-spacing and symmetric arrangement of atoms along the third dimension, a 3D visualization of the atomic structure is obtained based upon the atom counts. Slices have been generated along the $[1\bar{1}0]$ direction and stacked to visualize the structure in 3D as shown in Figure 4c. The cut planes represented by white lines in the figure indicate the orientation of $\{001\}$ and $\{111\}$ planes, and views along the respective orientations given in Figure 4d,e. In Figure 4d, the change in thickness of the wire from tip toward the center is clear. The presence of surface steps along with faceting is also evident from different viewing directions. A 360° rotation of the wire segment about different axes enables to identify the $\{001\}$ and $\{111\}$ facets (snapshots and movie in Supporting Information, Figures S4 and S5). The 3D visualization indeed confirms our interpretation on the wire structure: primarily the noncircular cross-sectional geometry and the surface morphology.

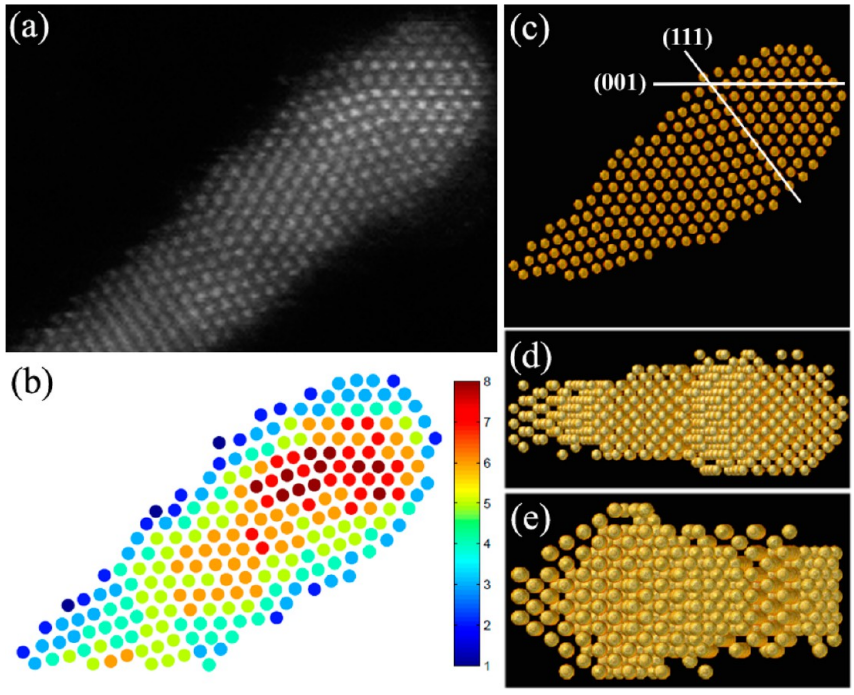

Figure 4. (a) High resolution HAADF-STEM image of a wire portion in $[1\bar{1}0]$ zone orientation, (b) showing the atom counts per atomic column. The computed 3D reconstruction of the wire obtained from the atom counts are given and presented from different views as in (c) $[1\bar{1}0]$ zone orientation with cut planes, represented by the white lines, indicating the orientation of the $\{001\}$ and $\{111\}$ planes; (d) [001] zone orientation and (e) [111] orientation.

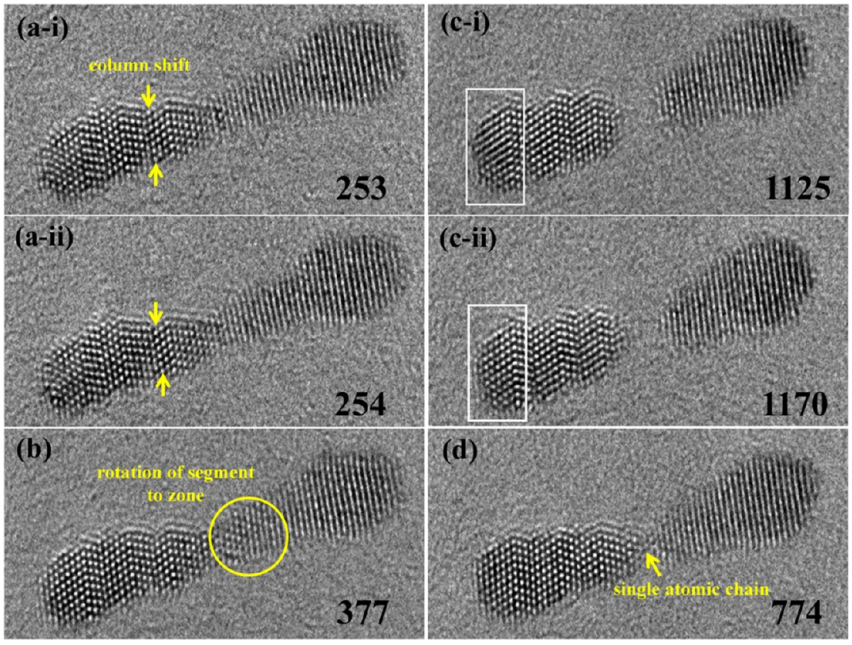

Figure 5. Snapshots extracted (frame no. mentioned at right corner of each image) from a movie (Supporting Information) showing the interaction of a wire with the electron beam until it broke. (a-i) and (a-ii) show two consecutive frames, in (a-ii) a single row of atomic columns has shifted by shear. The other frames describe several other key events that took place during interaction with the e-beam, before the wire broke into two separate segments. (b) A portion of wire appears in zone after rotation/atom displacements under the beam. (c) The two frames indicate a rotation of the tip of the wire and (d) possibly a single chain of atoms linking the two segments before breakage.

A more detailed atom dynamics study under the influence of the electron beam is carried out by increasing the dose to ~200 e/Å^2 s with an effective screen current of 2 nA. The wires break at several points under the beam, but it provides us information on the events that take place under the influence of electron beam (movie in Supporting Information, S6). Figure 5 illustrates a few frames extracted from the movie (recorded at 3 frames/s) to explain the key atomic changes that take place during the wire breaking. It shows the evolution of a 10 nm segment of 2 nm diameter, which undergoes several structural changes under the beam. A constant shearing motion of the {111} atomic planes is observed with exchange of atomic columns between adjacent planes as shown in Figure 5a(i,ii). The frame no. 254 (i) shows a row of 7 atomic columns that loses one column to the adjacent portion of wire and shifts the twin boundary by rotation of the portion on the right side (ii). It is interesting to note that the right portion of the wire is out of zone here which constantly rotates and comes in zone as in frame 377 in Figure 5b. This is noticeable for the few planes at the left tip of the wire as one goes from frame 1125 to 1170 in Figure 5c(i,ii). A short single atomic chain formation is identified in frame 774 (Figure 5d) which is interesting to note as it indicates that the wire breaks by constant shearing of the atomic planes and rotation with exchange of atomic columns unlike stretching along the length axis as reported earlier.[28]

These changes under the beam have important implications toward its mechanical behavior and provide a clear picture of the atom dynamics that might involve in the breaking and forming mechanism of the wires.[38] Also, this study shows the interaction of the wire with the electron beam which may have implications toward the structural changes undergone during electron transport in devices and the failure mechanism of the device element by electromigration. Moreover, the structure under low dose condition resembles the stable structure of these wires which has a rough surface with steps of few atoms indicating presence of numerous loosely coordinated atom sites and exposed facets which can contribute significantly to enhance its catalytic activity.[39,40] The strain in the surface is a considerable factor making it a potentially good catalyst for reactions like CO oxidation. The surface steps are also potential sites for molecular adsorption that is critical for analysis. Moreover, the presence of a large density of aperiodic twins, torsional strain at the twin boundaries and localized lattice strain in the wires, particularly in the outermost layer of atoms, could be a prime reason behind the unexpected transport behavior in these wires, reported recently, making them 'quantum wires'.

CONCLUSIONS

In conclusion, the external morphology and the internal atomic structure of gold nanowires of molecular dimension, synthesized at large scale *via* chemical

route, are investigated by aberration corrected electron microscopy. A combination of aberration corrected HR(S)TEM and reliable quantification methods has been used to understand the wire structure and bonding at atomic scale. It indicates a significant deviation from a perfect fcc configuration. These structural aspects for sure will have a strong influence on its electronic behavior. We also studied the atom dynamics as a result of its interaction with the electron beam. This clearly illustrates the breaking/forming mechanism of the wires and has far-reaching implications on their mechanical behavior and suitability in different fields of application.

EXPERIMENTAL SECTION

Wires Sample Preparation. A carbon film Cu grid was placed on a 1 cm × 1 cm glass slide and covered with Teflon tape to leave only a portion of carbon exposed to the reaction medium. This substrate was placed in the solution containing 2 mg $HAuCl_4$ complexed with 40 μL of oleyl amine in 5 mL of toluene medium. It was then heated to 95 °C and kept at the temperature for ~35 min. After cooling, the grid was taken out and cleaned in ethanol and dried. The grid was redipped in a fresh Au nanoparticles (~2 nm) colloid containing L-ascorbic acid and left at 40 °C for about an hour until the solution was purple in color. Grid was finally taken out and cleaned in ethanol, water and acetone before drying.

Microscopy. All imaging were performed on a TITAN^3 microscope equipped with an aberration corrector and operated at 120 kV for both TEM and STEM mode. To keep the low dose condition (approximately 20 e/Å^2 s), a screen current of 45 pA was used. Before STEM imaging, a mild O_2−Ar plasma cleaning step (30% power for 5 s, twice) was performed to ensure minimal carbon deposition under e-beam.

Conflict of Interest: The authors declare no competing financial interest.

Supporting Information Available: Image simulation, 3D visualization of wire, video of breaking of the wire under e-beam. This material is available free of charge *via* the Internet at http://pubs.acs.org.

Acknowledgment. S.V.A and S.T. gratefully acknowledge financial support from the Fund for Scientific Research Flanders (FWO). G.V.T. and P.K. acknowledge the ERC Grant N246791-COUNTATOMS. The microscope used in this study was partially financed by the Hercules Foundation of the Flemish Government. N.R. acknowledges the financial support from the Department of Science and Technology (DST).

REFERENCES AND NOTES

1. Grzelczak, M.; Perez-Juste, J.; Mulvaney, P.; Liz-Marzan, L. M. Shape Control in Gold Nanoparticle Synthesis. *Chem. Soc. Rev.* **2008**, *37*, 1783–1791.
2. Cademartiri, L.; Ozin, G. A. Ultrathin Nanowires—A Materials Chemistry Perspective. *Adv. Mater.* **2009**, *21*, 1013–1020.
3. Daniel, M.-C.; Astruc, D. Gold Nanoparticles: Assembly, Supramolecular Chemistry, Quantum-Size-Related Properties, and Applications toward Biology, Catalysis, and Nanotechnology. *Chem. Rev.* **2003**, *104*, 293–346.
4. Hutchings, G. J.; Brust, M.; Schmidbaur, H. Gold—An Introductory Perspective. *Chem. Soc. Rev.* **2008**, *37*, 1759–1765.
5. Chen, H.; Shao, L.; Li, Q.; Wang, J. Gold Nanorods and Their Plasmonic Properties. *Chem. Soc. Rev.* **2013**, *42*, 2679–2724.
6. Saha, K.; Agasti, S. S.; Kim, C.; Li, X.; Rotello, V. M. Gold Nanoparticles in Chemical and Biological Sensing. *Chem. Rev.* **2012**, *112*, 2739–2779.
7. Wang, B.; Yin, S.; Wang, G.; Buldum, A.; Zhao, J. Novel Structures and Properties of Gold Nanowires. *Phys. Rev. Lett.* **2001**, *86*, 2046–2049.
8. Roy, A.; Pandey, T.; Ravishankar, N.; Singh, A. K. Single Crystalline Ultrathin Gold Nanowires: Promising Nanoscale Interconnects. *AIP Adv.* **2013**, *3*, 032131.
9. Valden, M.; Lai, X.; Goodman, D. W. Onset of Catalytic Activity of Gold Clusters on Titania with the Appearance of Nonmetallic Properties. *Science* **1998**, *281*, 1647–1650.
10. Hammer, B.; Nørskov, J. K. Electronic Factors Determining the Reactivity of Metal Surfaces. *Surf. Sci.* **1995**, *343*, 211–220.
11. Bogozi, A.; Lam, O.; He, Li; Tao, N. J.; Nagahara, L. A.; Amlani, I.; Tsui, R. Molecular Adsorption onto Metallic Quantum Wires. *J. Am. Chem. Soc.* **2001**, *123*, 4585–4590.
12. He, H.; Tao, N. J. Interactions of Molecules with Metallic Quantum Wires. *Adv. Mater.* **2002**, *14*, 161–164.
13. Halder, A.; Ravishankar, N. Ultrafine Single-Crystalline Gold Nanowire Arrays by Oriented Attachment. *Adv. Mater.* **2007**, *19*, 1854–1858.
14. Lu, X.; Yavuz, M. S.; Tuan, H.-Y.; Korgel, B. A.; Xia, Y. Ultrathin Gold Nanowires Can Be Obtained by Reducing Polymeric Strands of Oleylamine−AuCl Complexes Formed *via* Aurophilic Interaction. *J. Am. Chem. Soc.* **2008**, *130*, 8900–8901.
15. Huo, Z.; Tsung, C.-K.; Huang, W.; Zhang, X.; Yang, P. Sub-Two Nanometer Single Crystal Au Nanowires. *Nano Lett.* **2008**, *8*, 2041–2044.
16. Feng, H.; Yang, Y.; You, Y.; Li, G.; Guo, J.; Yu, T.; Shen, Z.; Wu, T.; Xing, B. Simple and Rapid Synthesis of Ultrathin Gold Nanowires, Their Self-Assembly and Application in Surface-Enhanced Raman Scattering. *Chem. Commun.* **2009**, 1984–1986.
17. Kundu, P.; Chandni, U.; Ghosh, A.; Ravishankar, N. Pristine, Adherent Ultrathin Gold Nanowires on Substrates and Between Pre-Defined Contacts *via* a Wet Chemical Route. *Nanoscale* **2012**, *4*, 433–437.
18. Chandni, U.; Kundu, P.; Singh, A. K.; Ravishankar, N.; Ghosh, A. Insulating State and Breakdown of Fermi Liquid Description in Molecular-Scale Single-Crystalline Wires of Gold. *ACS Nano* **2011**, *5*, 8398–8403.
19. Qin, S.; Kim, T.-H.; Zhang, Y.; Ouyang, W.; Weitering, H. H.; Shih, C.-K.; Baddorf, A. P.; Wu, R.; Li, A.-P. Correlating Electronic Transport to Atomic Structures in Self-Assembled Quantum Wires. *Nano Lett.* **2012**, *12*, 938–942.
20. Hertel, T.; Walkup, R. E.; Avouris, P. Deformation of Carbon Nanotubes by Surface van der Waals Forces. *Phys. Rev. B* **1998**, *58*, 13870–13873.
21. Yang, L.; Han, J. Electronic Structure of Deformed Carbon Nanotubes. *Phys. Rev. Lett.* **2000**, *85*, 154–157.
22. Walsh, M. J.; Yoshida, K.; Kuwabara, A.; Pay, M. L.; Gai, P. L.; Boyes, E. D. On the Structural Origin of the Catalytic Properties of Inherently Strained Ultrasmall Decahedral Gold Nanoparticles. *Nano Lett.* **2012**, *12*, 2027–2031.
23. Van Tendeloo, G.; Bals, S.; Van Aert, S.; Verbeeck, J.; Van Dyck, D. Advanced Electron Microscopy for Advanced Materials. *Adv. Mater.* **2012**, *24*, 5655–5675.
24. Bals, S.; Van Aert, S.; Van Tendeloo, G.; Ávila-Brande, D. Statistical Estimation of Atomic Positions from Exit Wave Reconstruction with a Precision in the Picometer Range. *Phys. Rev. Lett.* **2006**, *96*, 096106.
25. Chandni, U.; Kundu, P.; Kundu, S.; Ravishankar, N.; Ghosh, A. Tunability of Electronic States in Ultrathin Gold Nanowires. *Adv. Mater.* **2013**, *25*, 2486–2491.
26. Rodrigues, V.; Ugarte, D. Metal Nanowires: Atomic Arrangement and Electrical Transport Properties. *Nanotechnology* **2002**, *13*, 404–408.
27. Oshima, Y.; Onga, A.; Takayanagi, K. Helical Gold Nanotube Synthesized at 150 K. *Phys. Rev. Lett.* **2003**, *91*, 205503.

28. Rego, L. G. C.; Rocha, A. R.; Rodrigues, V.; Ugarte, D. Role of Structural Evolution in the Quantum Conductance Behavior of Gold Nanowires During Stretching. *Phys. Rev. B* **2003**, *67*, 045412.
29. den Dekker, A. J.; Van Aert, S.; van den Bos, A.; Van Dyck, D. Maximum Likelihood Estimation of Structure Parameters from High Resolution Electron Microscopy Images. Part I: A Theoretical Framework. *Ultramicroscopy* **2005**, *104*, 83–106.
30. Van Aert, S.; den Dekker, A. J.; van den Bos, A.; Van Dyck, D.; Chen, J. H. Maximum Likelihood Estimation of Structure Parameters from High Resolution Electron Microscopy Images. Part II: A Practical Example. *Ultramicroscopy* **2005**, *104*, 107–125.
31. Van Aert, S.; Turner, S.; Delville, R.; Schryvers, D.; Van Tendeloo, G.; Salje, E. K. H. Direct Observation of Ferrielectricity at Ferroelastic Domain Boundaries in $CaTiO_3$ by Electron Microscopy. *Adv. Mater.* **2012**, *24*, 523–527.
32. Bals, S.; Casavola, M.; van Huis, M. A.; Van Aert, S.; Batenburg, K. J.; Van Tendeloo, G.; Vanmaekelbergh, D. I. Three-Dimensional Atomic Imaging of Colloidal Core–Shell Nanocrystals. *Nano Lett.* **2011**, *11*, 3420–3424.
33. Van Aert, S.; Batenburg, K. J.; Rossell, M. D.; Erni, R.; Van Tendeloo, G. Three-Dimensional Atomic Imaging of Crystalline Nanoparticles. *Nature* **2011**, *470*, 374–377.
34. Bals, S.; Van Aert, S.; Romero, C. P.; Lauwaet, K.; Van Bael, M. J.; Schoeters, B.; Partoens, B.; Yucelen, E.; Lievens, P.; Van Tendeloo, G. Atomic Scale Dynamics of Ultrasmall Germanium Cluster. *Nat. Commun.* **2012**, *3*, 1–6.
35. De Backer, A.; Martinez, G. T.; Rosenauer, A.; Van Aert, S. Atom Counting in HAADF STEM Using A Statistical Model-Based Approach: Methodology, Possibilities, and Inherent Limitations. *Ultramicroscopy* **2013**, *134*, 23–33.
36. Van Aert, S.; De Backer, A.; Martinez, G. T.; Goris, B.; Bals, S.; Van Tendeloo, G.; Rosenauer, A. Procedure to Count Atoms with Trustworthy Single-Atom Sensitivity. *Phys. Rev. B* **2013**, *87*, 064107.
37. Van Aert, S.; Verbeeck, J.; Erni, R.; Bals, S.; Luysberg, M.; Van Dyck, D.; Van Tendeloo, G. Quantitative Atomic Resolution Mapping Using High-Angle Annular Dark Field Scanning Transmission Electron Microscopy. *Ultramicroscopy* **2009**, *109*, 1236–1244.
38. da Silva, E. Z.; da Silva, A. J. R.; Fazzio, A. How Do Gold Nanowires Break? *Phys Rev. Lett.* **2001**, *87*, 256102.
39. Remediakis, I. N.; Lopez, N.; Nørskov, J. K. CO Oxidation on Rutile-Supported Au Nanoparticles. *Angew. Chem., Int. Ed.* **2005**, *44*, 1824–1826.
40. Rashkeev, S. N.; Lupini, A. R.; Overbury, S. H.; Pennycook, S. J.; Pantelides, S. T. Role of the Nanoscale in Catalytic CO Oxidation by Supported Au and Pt Nanostructures. *Phys. Rev. B* **2007**, *76*, 035438.